

## Theoretical exploration of the interference minimum in molecular high-order harmonic generation

Liqing Li, Yuanyuan Xu and Xiangyang Miao\*

*College of Physics and Information Engineering, Shanxi Normal University,  
Linfen 041004, China*

Received 8 August 2015; Accepted 10 September 2015

Published Online 1 March 2016

---

**Abstract.** The interference minimum in the molecular high-order harmonic generation is studied by numerically solving the non-Born-Oppenheimer approximation time-dependent Schrödinger equation. The results show that two kinds of interference minima appear in the high-order harmonic spectrum when the hydrogen molecular ion is exposed to the laser pulse. Furthermore, by adjusting wavelength of the laser as well as initial condition of nucleus, it is found that two kinds of interference minima are ascribed to the molecular structure and the electronic dynamics behavior induced by the laser field, respectively. Besides, the time-frequency distributions and the electron wave packet distributions are calculated to better understand the mechanism of the minimum.

**PACS:** 42.65.Ky, 33.80.Rv, 42.25.Hz

**Key words:** High-order harmonic generation, Interference minimum, Non-Born-Oppenheimer approximation

---

### 1 Introduction

Owing to the rapid advancement of laser technology, the dynamics of atoms or molecules exposed to an intense laser field [1-4] has become the subject of many theoretical and experimental investigations. Many nonlinear nonperturbative phenomena, such as charge resonance enhanced ionization (CREI) [5], above threshold ionization (ATI) [6] and high-order harmonic generation (HHG) [7, 8] have been discovered. In the past few years, high-order harmonic radiation has become a very active discussion in this field for the potential to produce ultrashort pulse (XUV) and X-ray source. The HHG process can be well understood by the semiclassical three-step model [9]: the electrons tunnel through

---

\*Corresponding author. Email addresses: sxxymiao@126.com (X.Y. Miao)

the barrier formed by the Coulomb potential and the laser field, then they oscillate in the laser field, and finally may recombine with the parent ion and emit a harmonic photon with energy equal to the ionization potential plus the kinetic energy of the recombining electron.

In recent years, molecular harmonic generation has been intensively investigated, since it contains more physical information than atom. On the one hand, as there are two or more nuclei in molecules, the returning electron experiences the two-center or multicenter potential, which induces the interference effect on the emission process of molecular HHG other than the atomic case. On the other hand, the molecular HHG is sensitive to the rotational [10] and vibrational motion [11] of nuclei, which provides a measuring means of molecular dynamics in intense laser field. For instance, Lein found that the harmonic spectra generated from the molecules would be approximately relevant to the nuclei vibrational autocorrelation function [11]. Furthermore, Feng *et al.* proved that the harmonic emissions from the  $H_2^+$  and  $D_2^+$  were sensitive to the initial vibrational state, with more intense harmonics generated in the lighter isotopes [12]. In addition, the main discovery in aligned molecular HHG spectra was the double-slit-type interference effect [13]. This interference effect was experimentally observed in aligned  $CO_2$  molecules by Kanai *et al.* [14] and this phenomenon was theoretically achieved in the simplest diatomic molecules  $H_2^+$  and  $H_2$  by Lein *et al.* [15]. Most of these studies indicate the importance of the nuclear motion and molecular structure in molecular dynamics. In fact, when molecules are irradiated by intense laser fields, it can be found that the interference effects have already appeared in many processes. To further research the interference effect which is caused by the molecular multicenter, the time-dependent Schrödinger equation (TDSE) is solved in this paper when a model  $H_2^+$  is exposed to an intense pulse. Numerical results show that the minimum in the low-order region is largely dependent on both the nuclear mass and the initial vibrational level, which demonstrates that the minimum in the low-order region mostly derives from molecular structure. In contrast, the minimum in the high-order region is strongly dependent on the fundamental wavelength, which indicates that this minimum is associated with the dynamic process caused by laser.

The rest of this paper is organized as follows. The numerical method in this work is presented in Sec. II. The results and discussions of interference effects are presented in Sec. III. The conclusion of our paper is given in Sec. IV. Atomic units are used throughout this paper unless stated otherwise.

## 2 Theoretical method

In this paper, the theoretical calculation adopts the one dimensional model that electron and two nuclei were fixed in a straight line. The HHG can be studied by numerically solving the non-Born-Oppenheimer approximation (NBOA) time-dependent Schrödinger equation via the parallel quantum wave-packet computer code LZH-DICP

[16-18]. In the dipole approximation and the length gauge, the TDSE for a molecule of  $\text{H}_2^+$  can be described as:

$$i\frac{\partial\Psi(R,z,t)}{\partial t}=\hat{H}(R,z,t)\Psi(R,z,t)=[T_R+Te+V_C(R,z)+V_I(z,t)]\Psi(R,z,t). \quad (1)$$

Among them,  $R$  is internuclear distance, and  $z$  is the electron coordinate (with respect to the nuclear center of mass).  $T_R = -\frac{1}{m_p}\frac{\partial^2}{\partial R^2}$  and  $T_e = -\frac{2m_p+1}{4m_p}\frac{\partial^2}{\partial z^2}$  denote the nuclear and the electronic kinetic-energy operator respectively, where  $m_p$  is the proton mass.  $V_c$  is the Coulomb potential of molecule  $\text{H}_2^+$ , which can be written as:

$$V_c(R,z)=\frac{1}{R}-\frac{1}{\sqrt{(z-R/2)^2+1}}-\frac{1}{\sqrt{(z+R/2)^2+1}}. \quad (2)$$

The external interaction  $V_I$  between the laser field and molecule reads:

$$V_I(z,t)=-\left(1+\frac{1}{2m_p+1}\right)zE(t). \quad (3)$$

The electric field of the driving laser is given by:

$$E(t)=E_0f(t)\cos(\omega t) \quad (4)$$

where  $\omega$  and  $E_0$  are the frequency of the fundamental laser pulses and the peak amplitudes, respectively. In the calculation, a function of the Gauss envelope is adopted:

$$f(t)=e^{-4\ln(2)t^2/\tau^2} \quad (5)$$

where  $\tau$  is full width of half-maximum.

The initial wave packet can be constructed by diagonalizing the field-free Hamiltonian. The time-dependent wave function is advanced using the standard second-order split-operator method [19-21]:

$$\Psi(R,z;t+\delta t)=e^{-iT\delta t/2}e^{-iV\delta t}e^{-iT\delta t/2}\Psi(R,z;t)+O(\delta t^3), \quad (6)$$

where  $\hat{T}$  is the kinetic energy operator and  $V$  is the interaction potential taking all the potential energy of the system plus a purely imaginary term to produce an absorbing boundary.

According to the Ehrenfest theorem [22], the time-dependent dipole acceleration can be calculated:

$$d_A(t)=\langle\Psi(R,z,t)|-\frac{\partial V_c}{\partial z}+E(t)|\Psi(R,z,t)\rangle. \quad (7)$$

The harmonic spectra are based on Fourier transforming the time-dependent dipole acceleration:

$$P_A(\omega)=\left|\frac{1}{\sqrt{2\pi}}\int_0^t d_A(t)e^{-i\omega t}dt\right|^2. \quad (8)$$

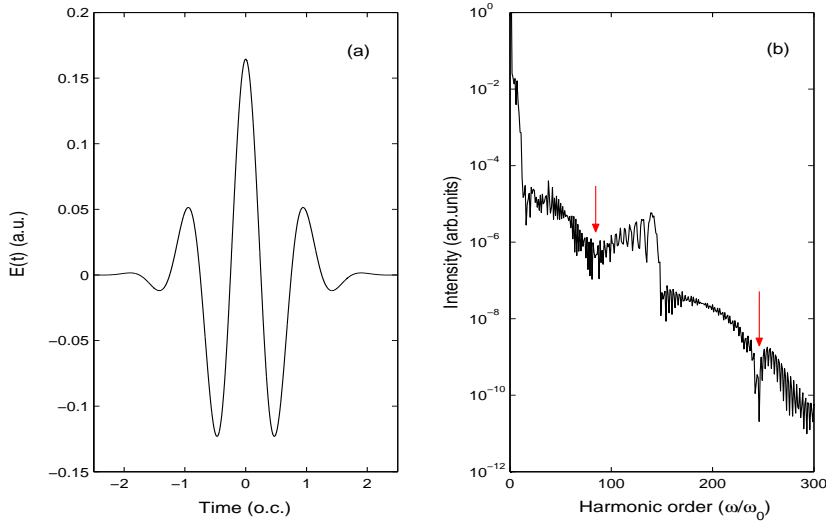


Figure 1: (a) and (b) are the sketch of laser field (1000 nm, 5 fs,  $9.5 \times 10^{14} \text{ W/cm}^2$ ) and the corresponding HHG spectrum of  $\text{H}_2^+$ , respectively.

To study the detailed spectral and temporal structures of HHG, the time-frequency analysis is performed by means of the wavelet transform [23]:

$$d_\omega(t) = \int d_A(t') \sqrt{\omega} W[\omega(t' - t)] dt'. \quad (9)$$

The mother wavelet is given by the Morlet wavelet [24]:

$$W(x) = \frac{1}{\sqrt{\tau}} e^{ix} \exp\left(\frac{-x^2}{2\tau^2}\right). \quad (10)$$

### 3 Results and discussion

In Fig. 1, the laser field (5 fs, 1000 nm,  $9.5 \times 10^{14} \text{ W/cm}^2$ ) and the corresponding harmonic spectrum of  $\text{H}_2^+$  with initial vibrational state equal to zero ( $v = 0$ ) are presented, respectively. As shown in Fig. 1(b), the harmonic spectrum of  $\text{H}_2^+$  exhibits a plateau following the quick decrease for harmonics lower than the 150th order and a sharp cutoff at about the 260th order. In addition, from the figure it can be clearly seen that two minima exist in the low-order region and the high-order region (marked by the arrow), respectively. Compared the harmonic spectrum in Fig. 1(b) with the atomic harmonic spectra, the principal difference between them is that the former appears the destructive interference in the plateau. Because the dynamics of the HHG for the molecular systems are much more complex than that for the atomic systems, it can be inferred that the minima may well originate from molecular structure or be caused by other factors.

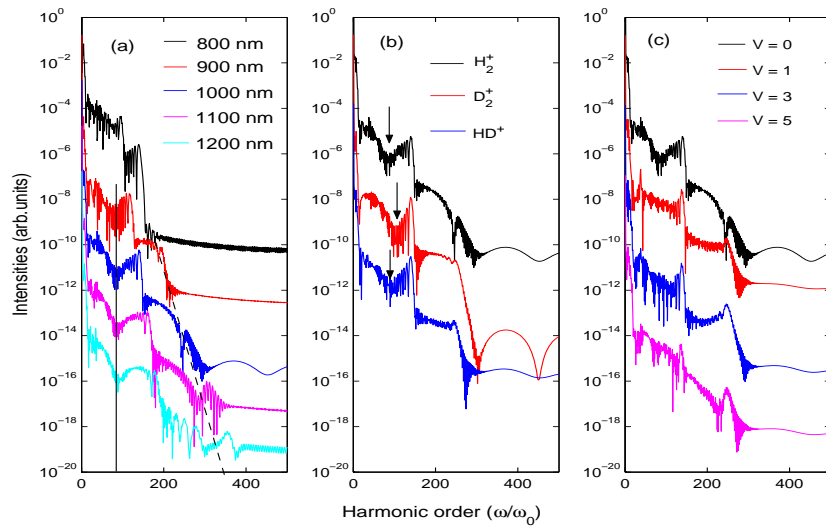


Figure 2: (a) The HHG spectra of  $\text{H}_2^+$  taken at the wavelengths of 800 nm (black line), 900 nm (red line), 1000 nm (blue line), 1100 nm (magenta line), 1200 nm (cyan line), respectively, from top to bottom. (b) The HHG spectra of  $\text{H}_2^+$  (black curve),  $\text{D}_2^+$  (red curve) and  $\text{HD}^+$  (blue curve) under the 1000 nm laser pulse, respectively. (c) The HHG spectra from the different initial vibrational states of the  $\text{H}_2^+$  ( $v = 0, 1, 3$  and 5) under the 1000 nm laser pulse. The harmonic intensities have been multiplied by factors of 1,  $10^{-3}$ ,  $10^{-6}$ , and so on from top to bottom for the purpose of clarity. In all above cases, the duration of the laser pulse is 5 fs, and the peak intensity of the pulse is  $9.5 \times 10^{14} \text{ W/cm}^2$ .

To clarify the mechanism of the interference minima, the different harmonic spectra from  $\text{H}_2^+$  are calculated by changing the wavelength of driving laser pulse in a few-cycle laser pulse with duration of 5 fs and peak intensity of  $9.5 \times 10^{14} \text{ W/cm}^2$ . The calculated harmonic spectra with the wavelengths of 800 nm, 900 nm, 1000 nm, 1100 nm, 1200 nm are displayed in Fig. 2(a). One can find that there is still the destructive interference in the plateau except for 800 nm. Clearly, the location of the interference minimum (marked by the straight line) in the low-order region almost keeps invariant, but the position of minimum (marked by the dotted line) in the high-order region is observably changed, with the changing of driving laser wavelength. Then it can be considered that there may be different physical mechanism between the two kinds of minima.

Previous research [25] has already proved that the process of HHG can be impacted obviously by the nuclear motion and nuclear mass, which are maybe the key factors of the interference minimum mentioned above. So the mechanism of the minimum is investigated by adjusting the initial condition of nucleus in the following work. The HHG spectra of  $\text{H}_2^+$  and its isotopic variant  $\text{D}_2^+$ / $\text{HD}^+$  at  $v = 0$  are shown in Fig. 2(b) in the case of the 1000 nm laser field. It is clear that the spectra of  $\text{H}_2^+$  and  $\text{D}_2^+$ / $\text{HD}^+$  share the same features: the first few harmonics present a fast decreases, then followed by the first plateau, finally they cut off through the second plateau where all the harmonics have the same strength. Moreover, the spectra of  $\text{D}_2^+$ / $\text{HD}^+$  also present the destructive

interference in the first plateau. However, the distinct difference also exists among the three cases. The interference minima (marked by the arrow) are located around the 85th, 110th and 100th for  $H_2^+$ ,  $D_2^+$  and  $HD^+$  respectively. Compared the harmonic spectra in Fig. 2(a) with those in Fig. 2(b), the position of the minimum in the low-order region is more sensitive to the nuclear mass than the wavelength of the laser, which implies that such a minimum is probably caused by the structure of molecules themselves rather than by the electronic dynamics behavior induced by the laser field.

In order to give a deeper insight into the mechanism of the interference minimum mentioned above, the effect of the initial vibrational level on the interference minimum for the  $H_2^+$  with the same laser parameters as Fig. 1 is investigated. The HHG spectra of  $H_2^+$  at different initial vibrationl levels ( $v = 0, 1, 3$  and  $5$ ) are provided in Fig. 2(c). One can clearly see that a remarkable interference minimum around the 85th order appears in the harmonic spectrum of  $H_2^+$  at  $v = 0$ , while there is no very conspicuous dip at about the 85th in the harmonic spectra of  $H_2^+$  at  $v = 1, v = 3, v = 5$ , respectively. Obviously, with the increase of initial vibrational level, the interference minimum weakens distinctly around the 85th in the low-order region. As far as we know, the internuclear separation tends to increase with the increase of the initial vibrational level. And then it opens and enlightens us that the increase of the internuclear separation may be a key factor to affect the interference minimum. Like the description in the Fig. 5 in Ref. [15], for lower harmonic orders, the minimum structure at higher internuclear separation becomes irregular and relatively flat. A possible reason is that HHG at lower orders is complicated by transitions from continuum states into excited states [15]. Accordingly, it is reasonable that the increase of initial vibrational state is responsible for the weakening of interference minimum in the low-order region in Fig. 2(c). That is to say, for lower harmonic orders, the interference minimum is sensitive to the internuclear separation. Hence, it is further demonstrated that the interference minimum in the low-order region is ascribed to the molecular structure.

In the following part, it is worthy to notice the interference minimum in the high-order region. The temporal profiles of the 900nm and the 1200nm laser fields are presented in Figs. 3(a) and (c) respectively, and the quantum time-frequency analyses in both cases are adopted to investigate the related physical mechanism. The corresponding results are presented in Figs. 3(b) and 3(d). One can obviously see that there are two main photon-energy peaks, marked as  $P_1$  and  $P_2$  for the two cases, respectively. The two peaks indicate the maximum emitted energy of the returning electrons, as well as their recombination times in each half-cycle emission. At the same time, the cancellations around the 85th order marked by the white arrow in Figs. 3(b) and (d) are also observed clearly, which is well according with the interference minima in the low-order region shown in Fig. 2(a). However, it is important to note that the considerable suppression of harmonic emission occurred around time  $t = 0.1$  optical cycle (o.c.) (marked by the red arrow) is significantly shown in Fig. 3(d) for the 1200 nm case as compared with that shown in Fig. 3(b) for the 900 nm case. This result agrees well with the interference minimum in the high-order region in Fig. 2(a), in which it can be found that the interference minimum

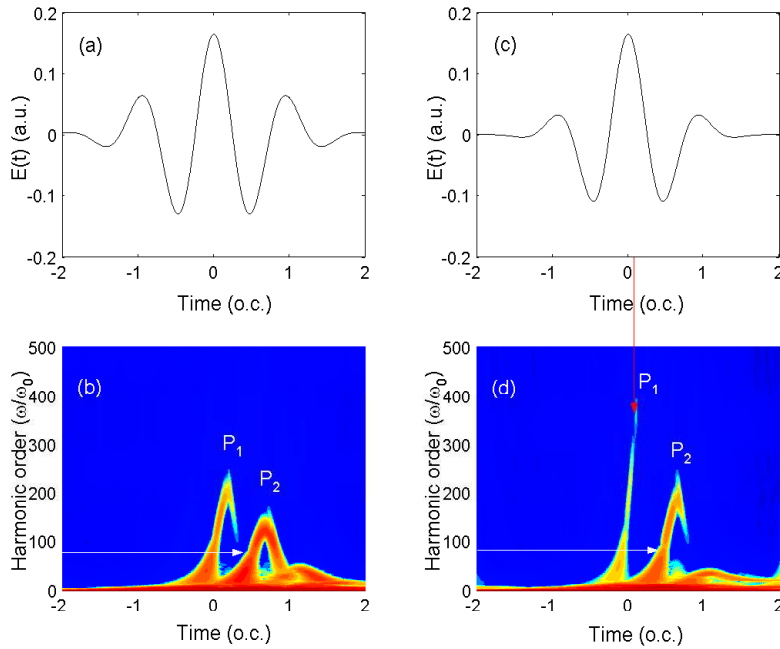


Figure 3: (a) and (b) The profile of the laser field and the corresponding time-frequency distribution in the case of 900 nm pulse. (c) and (d) The results in the case of 1200 nm pulse. The other parameters are identical to those in Fig. 1.

significantly appears in the high-order region for the case of 1200 nm instead of 900 nm.

To obtain clear insight, the time-dependent electronic probability density distributions are presented in Figs. 4(a), (b), (c) and (d), respectively. In all above cases, the electronic density distributions are practically similar. It can be obviously seen that the electronic wave packets periodically scatter between the two nuclei during interacting with the intense laser pulse. It can be obviously seen that the electronic wave packets periodically scatter between the two nuclei during interacting with the intense laser pulse. Nevertheless, some apparent differences can be still observed. For instance, at about  $t = 0.1$  o.c. (marked by the arrow), the population of electrons shown in Figs. 4(b), 4(c) and 4(d) for the cases of 1000 nm, 1100nm and 1200nm laser pulses is more than that shown in Fig. 4(a) for the case of 900 nm laser pulse. In the following discussion, the cases of 900 nm and 1200 nm laser pulses are compared and the corresponding physical mechanism is further investigated. Based on the former research [26], it can be learned that the electron wave packet distribution is strongly dependent on the changes of combined Coulomb and laser field potential when the molecule is exposed to an intense laser field. As almost identical strength of external electric field around  $t = 0.1$  o.c. shown in Figs. 3(a) and (c) for the 900nm and 1200 nm cases, the potential wells in both cases at this time are nearly same with each other, meaning that the effect of combined Coulomb

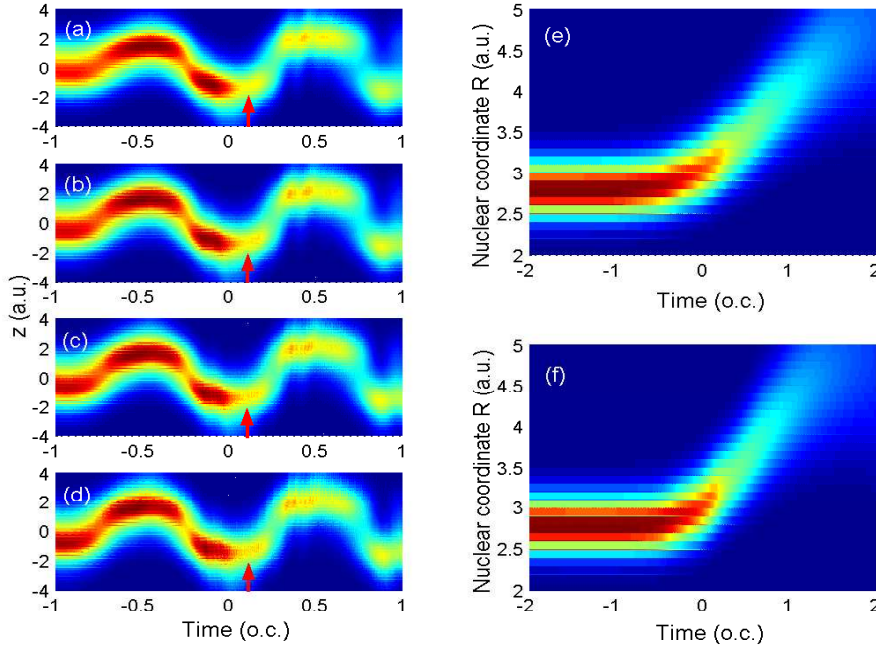


Figure 4: (a)-(d) The time-dependent electron density distributions for the 900 nm, the 1000 nm, the 1100 nm, and the 1200 nm laser fields, respectively. The time evolution of the nuclear probability densities of  $\text{H}_2^+$  for the 900 nm (e) and the 1200 nm (f) laser fields. The other parameters are the same as those in Fig. 1.

and laser field potential on the electron wave packet distribution can be omitted. Then, one can be deduced that the difference of the population of electrons (around  $t = 0.1$  o.c.) between the above two cases may be decided by the numbers of the ionized electrons. It is well known that the ionization process for the molecular ion in intense laser pulse can be affected by the electric field strength and the internuclear separation. To study the ionization processes of the two cases, the nuclear wave packets of  $\text{H}_2^+$  for the 900 nm and the 1200 nm cases are displayed in Figs. 4(e) and 4(f), respectively. It can be obviously seen that the wave packets in both cases extend to the nearly same internuclear distance during interacting with the intense laser field. Therefore, the effects of the electric field strength and the internuclear separation on the ionization process around  $t = 0.1$  o.c. can be neglected. Accordingly, it can be considered that the difference of ionization process between the two cases may be caused by other factors. Then, it can understand that there may be collisions between the recollision electrons and the bound electrons in critical situation (i.e., the bound electrons will be ionized) at about  $t = 0.1$  o.c. for the 1200 nm case, so it is difficult for the bound electrons to be ionized, resulting in more electrons located around the nucleus under this condition. According to the three-step model [9], the interference effects occur in the recombination process of HHG, so the direction of velocity of returning electron may play a significant role in the interference process. And for all

we know, the considerable suppression of harmonic emission occurs at times when the continuum electron and bound electron have opposite average velocities [27]. As a consequence, it is reasonable that there is a conspicuous cancellation of trajectory (returning around  $t = 0.1$  o.c.) in the high-order region in the 1200 nm case as shown in Fig. 3(d). That is to say, the suppression of harmonic emission strongly correlates with the direction of velocity of returning electron for the cases of 1000 nm, 1100 nm and 1200 nm. Based on the discussion above mentioned, the suppression of harmonic emission in the high-order region for the 1000 nm, 1100 nm and 1200 nm cases occurs at nearly the same optical cycle (around  $t = 0.1$  o.c.). However, with the increase of laser wavelength, the returning electrons gain more energy from the laser field due to the long traveling time of electrons in the continuum, thus the corresponding position of the cancellation of trajectory (returning around  $t = 0.1$  o.c.) will increases to the higher harmonic. Hence, it is reasonable that the position of the interference minimum in the high-order region is observably changed for the conditions of different wavelengths as shown in Fig. 2(a). That is to say, the position of minimum in the high-order region is sensitive to the wavelength of the laser. As a result, taken these factors into consideration, it indicates that the interference minimum in the high-order region is due to the electronic dynamics behavior induced by the laser field.

## 4 Conclusion

In conclusion, the interference minima in the HHG have been theoretically investigated when the  $H_2^+$  is exposed to an intense pulse. By numerically solving the non-Born-Oppenheimer approximation time-dependent Schrödinger equation, the high-order harmonic spectra under the different conditions can be obtained, and the interference effects in the emission process of HHG are deeply studied. As a result, with the laser wavelength changing, the location of the interference minimum in the low-order region keeps invariant. Furthermore, the isotopes of  $H_2^+$  and the initial vibrational state play important roles in modulating the interference minimum. On the one hand, with the nuclear mass varying, the position of minimum in the low-order region also changes. On the other hand, with the increase of initial vibrational level, the interference minimum in the low-order region weakens apparently for the  $H_2^+$ . It demonstrates that this minimum is due to the molecular structure. In contrast, as the result of the cancellation of returning trajectory due to the collisions between the recollision electrons and the bound electrons, the interference minimum appears in the high-order region and the position of minimum is sensitive to the wavelength of the laser. It indicates that the minimum in the high-order region is due to the electronic dynamics behavior induced by the laser field.

**Acknowledgments.** The authors sincerely thank Prof. Keli Han and Dr. Ruifeng Lu for providing us the LZH-DICP code. This work is supported by the National Natural Science Foundation of China (Grant No. 11404204), Key Project of Chinese Ministry of

Education (Grant No. 211025), Research Fund for the Doctoral Program of Higher Education of China (Grant No. 20111404120004) and the Natural Science Foundation for Young Scientists of Shanxi Province, China (Grant No. 2009021005).

## References

- [1] F. Krausz and M. Ivanov 2009 Rev. Mod. Phys. 81 163.
- [2] Y. Wu and X. X. Yang 2007 Phys. Rev. A 76 013832.
- [3] Y. Wu and X. X. Yang 2007 Phys. Rev. Lett. 98 013601.
- [4] A. T. Le, T. Morishita, R. R. Lucchese *et al.* 2012 Phys. Rev. Lett. 109 203004.
- [5] T. Zuo and A. D. Bandrauk 1995 Phys. Rev. A 52 R2511.
- [6] G. G. Paulus, F. Lindner, H. Walther *et al.* 2003 Phys. Rev. Lett. 91 253004.
- [7] H. N. Du and X. Y. Miao 2012 Spec. Lett. 45 556.
- [8] Y. H. Wang, H. P. Wu, Y. Chen *et al.* 2012 AIP ADVANCES 2 022102.
- [9] P. B. Corkum 1993 Phys. Rev. Lett. 71 1994.
- [10] S. Ramakrishna and T. Seideman 2007 Phys. Rev. Lett. 99 113901.
- [11] M. Lein 2005 Phys. Rev. Lett. 94 053004.
- [12] L. Q. Feng and T. S. Chu 2012 J. Chem. Phys. 136 054102.
- [13] M. Lein, N. Hay, R. Velotta *et al.* 2002 Phys. Rev. Lett. 88 183903.
- [14] T. Kanai, S. Minemoto and H. Sakai 2005 Nature (London) 435 470.
- [15] M. Lein, N. Hay, R. Velotta *et al.* 2002 Phys. Rev. A 66 023805.
- [16] H. X. He, R. F. Lu, P. Y. Zhang *et al.* 2011 Phys. Rev. A 84 033418.
- [17] M. Lein, T. Kreibich, E. K. U. Gross *et al.* 2002 Phys. Rev. A 65 033403.
- [18] R. F. Lu, P. Y. Zhang and K. L. Han 2008 Phys. Rev. E 77 066701.
- [19] J. Hu, K. L. Han and G. Z. He 2005 Phys. Rev. Lett. 95 123001.
- [20] J. A. Fleck, J. R. Morris and M. D. Feit 1976 Appl. Phys. A 10 129.
- [21] R. F. Lu, T. S. Chu and K. L. Han 2005 J. Phys. Chem. A 109 6683.
- [22] K. Burnett, V. C. Reed, J. Cooper *et al.* 1992 Phys. Rev. A 45 3347.
- [23] X. M. Tong and Sh. I. Chu 2000 Phys. Rev. A 61 021802(R).
- [24] X. Chu and Sh. I. Chu 2001 Phys. Rev. A 64 021403(R).
- [25] X. Y. Miao and H. N. Du 2013 Phys. Rev. A 87 053403.
- [26] X. Y. Miao and C. P. Zhang 2014 Phys. Rev. A 89 033410.
- [27] T. Bredtmann, S. Chelkowski and A. D. Bandrauk 2011 Phys. Rev. A 84 021401(R).